2022

A Cambrian U-Pb age for the Mewstone Granite, SW Tasmania

Author: J. L. Everard and S. Meffre
Date: 2/11/2022
Email: info@mrt.tas.gov.au
Website: www.mrt.tas.gov.au

REPORT No.: TR33

Geological Survey Technical Report 33

Tasmanian Government

Mineral Resources Tasmania
Department of State Growth

Geological Survey Technical Report 33:

A Cambrian U-Pb age for the Mewstone Granite, SW Tasmania

by J. L. Everard and S. Meffre

Cover: The Mewstone, view from the northwest. (photo: Micah Visoiu)

Abstract

Eleven zircon grains extracted from a sample of the Mewstone Granite yielded a best estimate age of 495.6 ± 5.2 Ma (Cambrian: Furongian), based on $^{238}U/^{206}Pb$ (LA-ICPMS) with correction for common lead. The age is within error of that of the similar South West Cape Granite. Both bodies are coeval with several other western Tasmanian sub-volcanic granites that were emplaced during the waning phase of Mt Read Volcanics magmatism. They differ from them in their more peraluminous "S-type" composition and may represent a more distal phase of that magmatism, in which granitic magmas assimilated sedimentary material as they were emplaced into the adjacent Proterozoic basement.

Tasmanian Government

Mineral Resources Tasmania

Department of State Growth
www.mrt.tas.gov.au

A Cambrian U-Pb age for the Mewstone Granite, SW Tasmania

by J. L. Everard[1] and S. Meffre[2]
[1]*Geological Survey Branch - Mineral Resources Tasmania*
[2]*School of Natural Sciences - University of Tasmania*

CONTENTS

FIGURES

APPENDICES

1.0 INTRODUCTION

The Mewstone Granite is one of three small bodies of outcropping granite in far southwest Tasmania (Fig. 1). It forms the Mewstone (Fig. 2), a small (~13 ha) island which rises steeply to about 150 m asl, located 22 km south of the nearest point on the Tasmanian mainland and 12 km SE of Maatsuyker Island (43°44'18''S, 146°22'22''E). Black et al. (2005) showed that the other bodies, the South West Cape Granite and Cox Bight Granite, are Cambrian and Devonian in age respectively, but the granite composing the Mewstone has not previously been dated. The main purpose of this report is to document a U-Pb age obtained from zircon from the Mewstone. Petrographic and geochemical data are also presented and compared with those from other southwest Tasmanian granites.

2.0 PREVIOUS WORK

The geology and geomorphology of the Mewstone have previously been described by Banks (1993) and its topography and limited biota are most recently described by Brothers et al. (2001).

Banks (1993) examined rock specimens and photographs and noted that the island and several nearby islets and stacks are composed entirely of granite, characterised by closely spaced (<1 m) jointing (Fig. 3). He described in detail four specimens of granite and two of quartz veins. The granite is "medium-light grey (N6) with a few quartz and feldspar grains up to 7 mm long, in a finer-grained groundmass… In thin section, quartz, K-feldspar [microcline], plagioclase [albite], microperthite and rosettes and crystals of muscovite can be recognised.... Graphic intergrowth (cuneiform texture)

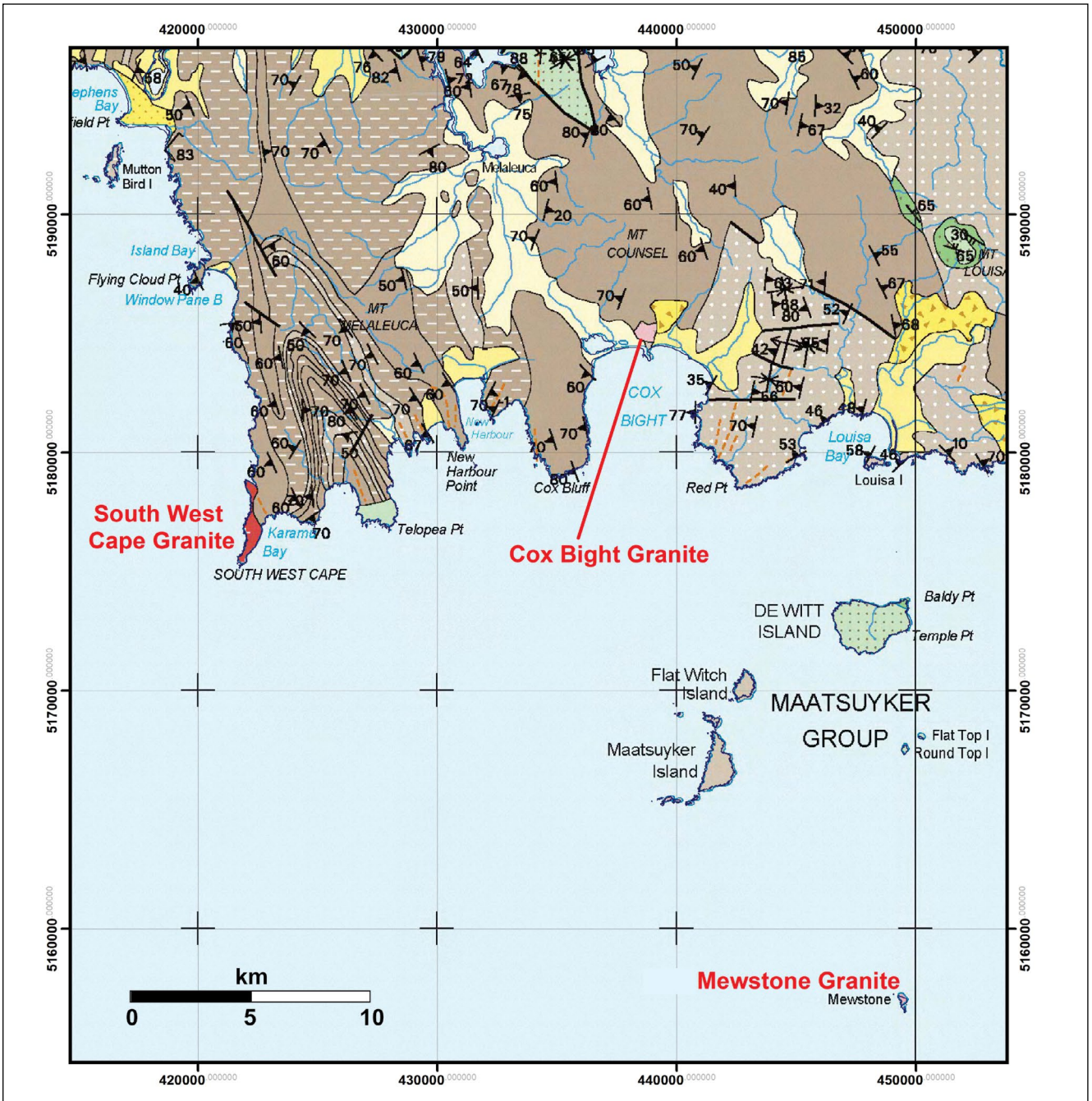

Figure 1. Location map of the Mewstone, showing regional geology (from MRT 1:250000 digital data) with other granite bodies labelled. Brown: Mesoproterozoic metasediments; green: Cambrian sedimentary rocks; red and pink: granites.

Figure 2. View of the Mewstone from the south; Tasmanian mainland in distance. (Photo: Micah Visoiu)

Figure. 3. Detail of granite outcrop, the Mewstone. Note close-spaced vertical jointing. (Photo: Micah Visoiu)

of quartz and feldspar is common, in places spectacular." Tourmaline, sometimes with inclusions of rutile and possibly ilmenite, and greenish biotite were reported in some sections. Cavities lined successively with feldspar, quartz and phosphate, veins of quartz and/or phosphate, and a surface film probably also of phosphate, were also noted.

3.0 PETROGRAPHY

Three samples (70937, 66272B and 66270) of granite and another (66273B) of a quartz vein were borrowed from the collection of the Geology Department (now School of Natural Sciences), University of Tasmania.

Three new thin sections of the sample (70937) used for dating were prepared in the Mineral Resources Tasmania (MRT) laboratories. They consist of a ± equigranular mosaic of clear quartz anhedra (mostly 400 μm – 1 mm with a few grains up to 2.5 mm, and one of 7 mm) and turbid anhedra and subhedra of partly sericitized alkali feldspar of similar dimensions (Fig. 4). Textures and twinning of feldspar is partly obscured by alteration, but microperthitic intergrowths are common and albite and, less commonly, microcline twinning can be recognised (Fig. 5). There are small interstitial patches of micrographic quartz-feldspar intergrowths, and fine-grained colourless muscovite (<<1 %). Rare, ragged flakes of biotite (≤ 500 um) retain some pleochroism (grey-brown to colourless) in places, but are largely altered to a turbid aggregate of muscovite and finely acicular opaques.

Another sample (66272B) is similar, although with a greater volume (1 – 2 vol%) of muscovite which forms interstitial rosettes between feldspar grains (Fig. 6). Micrographic quartz feldspar intergrowths are particularly well-developed (Figs. 6, 7). Sample 66270 is similar, with better preserved twinning of feldspars, and possible pseudomorphs after biotite, replaced by very fine-grained pale brown sericite.

Minute grains of possible chalcopyrite were noted in the coarser-grained quartz-rich vein rock (66273B).

Zircons (≤ 40 μm) are present in several samples and separation and analysis (by LA-ICPMS) of these grains provided a means of dating this body.

4.0 GEOCHEMISTRY

An off-cut of the dated sample (70937) was analysed in the MRT laboratories using standard X-ray fluorescence (XRF) techniques for both major and trace elements, with Fe_2O_3/FeO determined by $KMnO_4$ titration. Some of the remaining powder was also analysed by XRF at Geoscience Australia, where trace elements were also determined by inductively coupled plasma mass spectroscopy (ICPMS). Results from the various labs and methods are in excellent agreement (Table 1; Appendix 1).

The sample is a very felsic, quite peraluminous granite with very low MgO (0.07%), CaO (0.06%) and TiO_2 (0.10%). This, together with high Rb (311 ppm) and low Sr (13 ppm) and Ba (29 ppm), consistent with feldspar fractionation, indicates that it is a strongly fractionated granite. It is also moderately peraluminous, with ASI (Alumina Saturation Index) of ~1.16 – 1.22 (two analyses, Table 1; Appendix 1). In the terminology of Chappell and White (1974, 1992), derived mainly from Palaeozoic granites from the Lachlan Fold Belt, the Mewstone Granite is therefore an S-type (i.e. derived from partial melting of a dominantly sedimentary protolith). Other features characteristic of strongly fractionated S-types (e.g. Sawka et al., 1990; Chappell & White, 1992; Wyborn & Chappell, 1998; Chappell, 1999) are high P_2O_5 (0.39, 0.45%) and low levels of Y, rare earth elements (REE), Th and most high field strength elements. This is related to the greater solubility of phosphorus in strongly peraluminous melts (e.g. Pichavant et al. 1992; Wolf & London 1994); apatite crystallisation is delayed, bur REE-Y-Th phosphates crystallise early, depleting the melt in these elements (e.g. Montel, 1986).

Petrographic features, however, in particular the sericitization of feldspar, suggest the possible loss of some CaO and Na_2O due to alteration, which would increase apparent ASI. The rock contains insufficient CaO to account for all P_2O_5 as apatite, and another phosphorus-bearing phase must be present. This situation has been reported in the strongly peraluminous Interview Suite of western Tasmania, in which the apatite crystals have high Mn contents (Wyborn & Chappell, 1998). In the Mewstone Granite, however, some of the excess P_2O_5 may be of organic origin, as Banks (1993) noted phosphate in cavities and possibly surface films.

The chondrite normalised REE pattern of the Mewstone Granite (Fig. 8) is characterised by nearly flat light- and middle REE at relatively low levels (~10 x chondrite), a large negative Eu anomaly, and strong depletion of heavy REE (to less than chondrite for Yb). The convex shape of the La-Ce-Pr-Nd and Gd-Tb-Ho-Er segments can be attributed to the lanthanide tetrad effect, which in this context suggests exchange of REE with a high temperature aqueous fluid, i.e. hydrothermal alteration (e.g. McLennan, 1994; Masuda et al., 1987). The extreme negative Eu anomaly (Fig. 8) and non-chondritic ratios of Y/Ho (~39) and Zr/Hf (~22.5) of the Mewstone Granite are also consistent with interaction with a hydrothermal fluid. In this situation, in the final stages of granite crystallisation, partitioning of trace elements

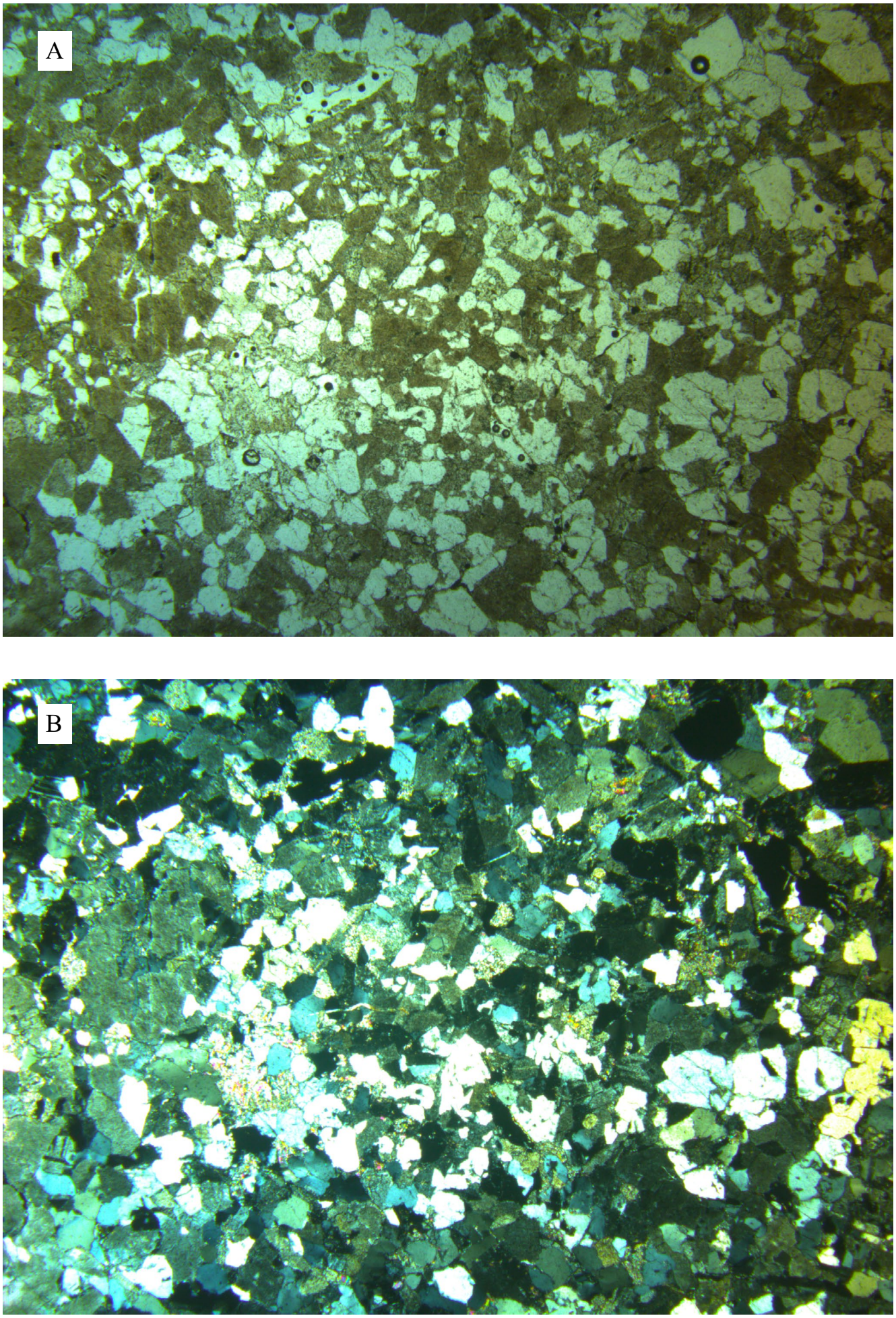

Figure 4. Photomicrograph of sample 70937, field of view ~9.8 x 7.3 mm. a) Plane polarised light; quartz clear, sericitized feldspar brown. b) Crossed nicols.

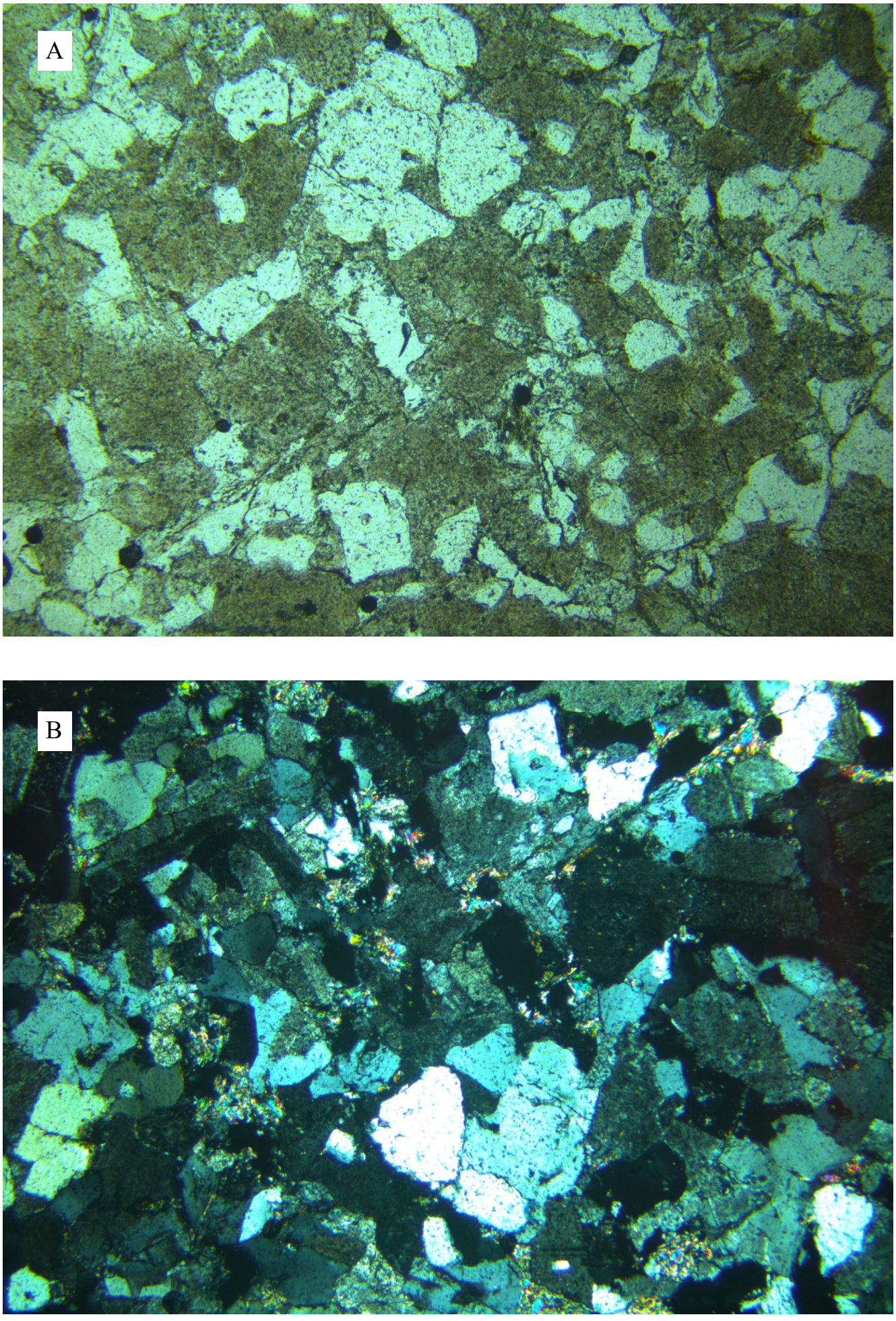

Figure 5. Photomicrograph of sample 70937, field of view ~4.6 x 3.4 mm. a) Plane polarised light. b) Crossed nicols; note twinning of feldspars and interstitial muscovite (high birefringence).

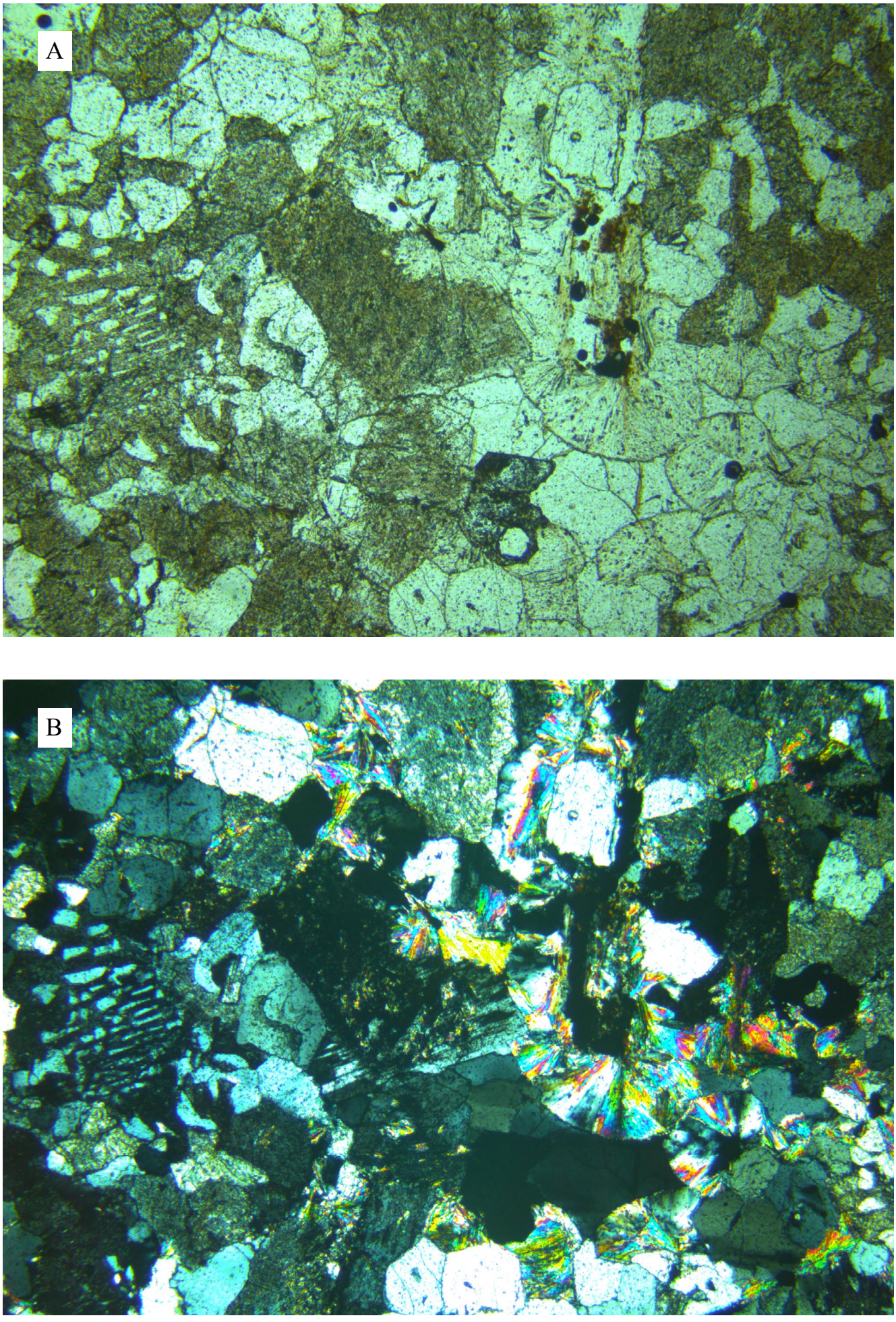

Figure 6. Photomicrograph of sample 66272B, field of view ~4.6 x 3.4 mm. a) Plane polarised light; note micrographic quartz-feldspar intergrowth (far left) and radiating sheaves of muscovite (lower right). b) Crossed nicols.

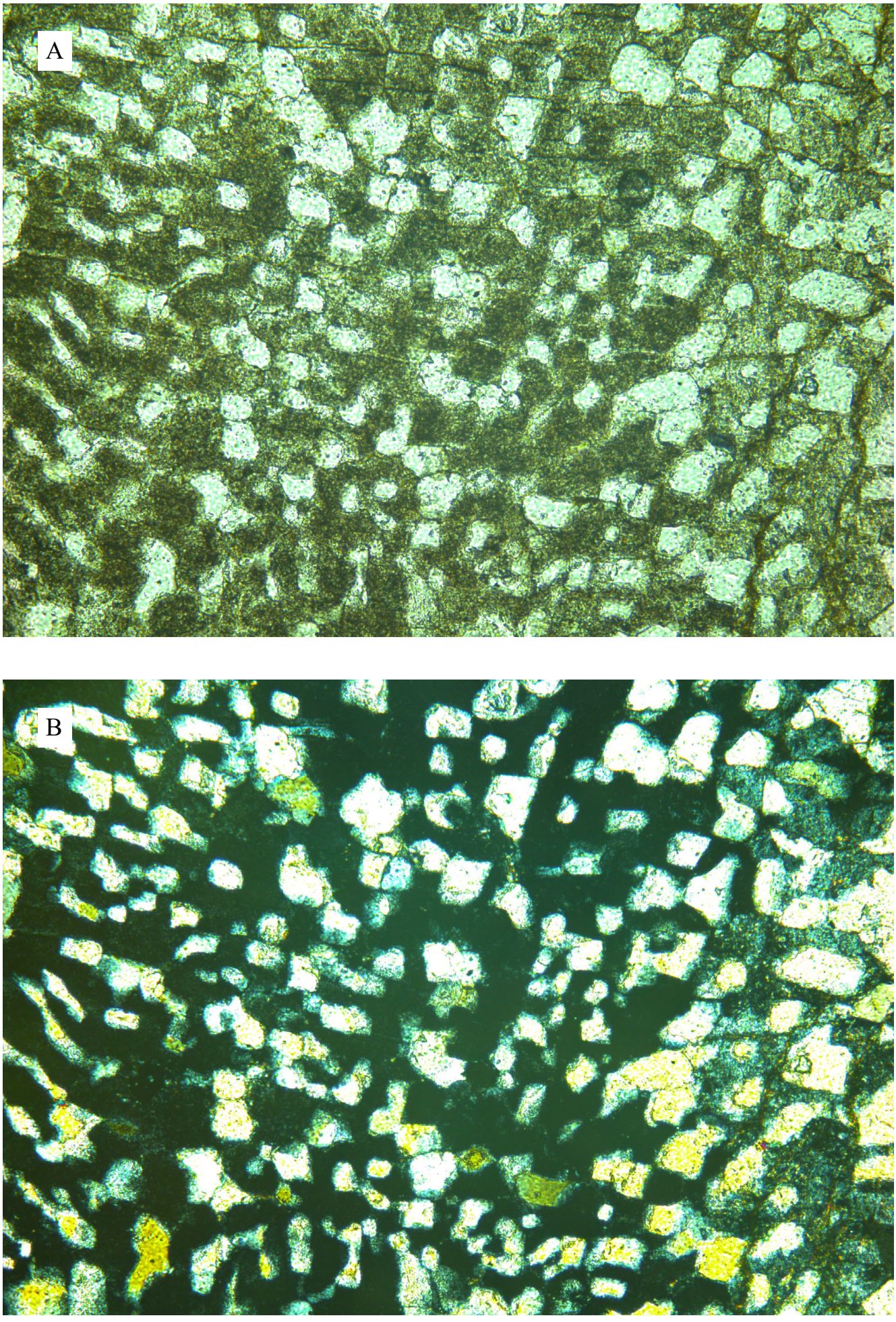

Figure 7. Photomicrograph of sample 66272B, field of view ~1.9 x 1.4 mm. Detail of micrographic quartz-feldspar intergrowth. a) Plane polarised light. b) Crossed nicols.

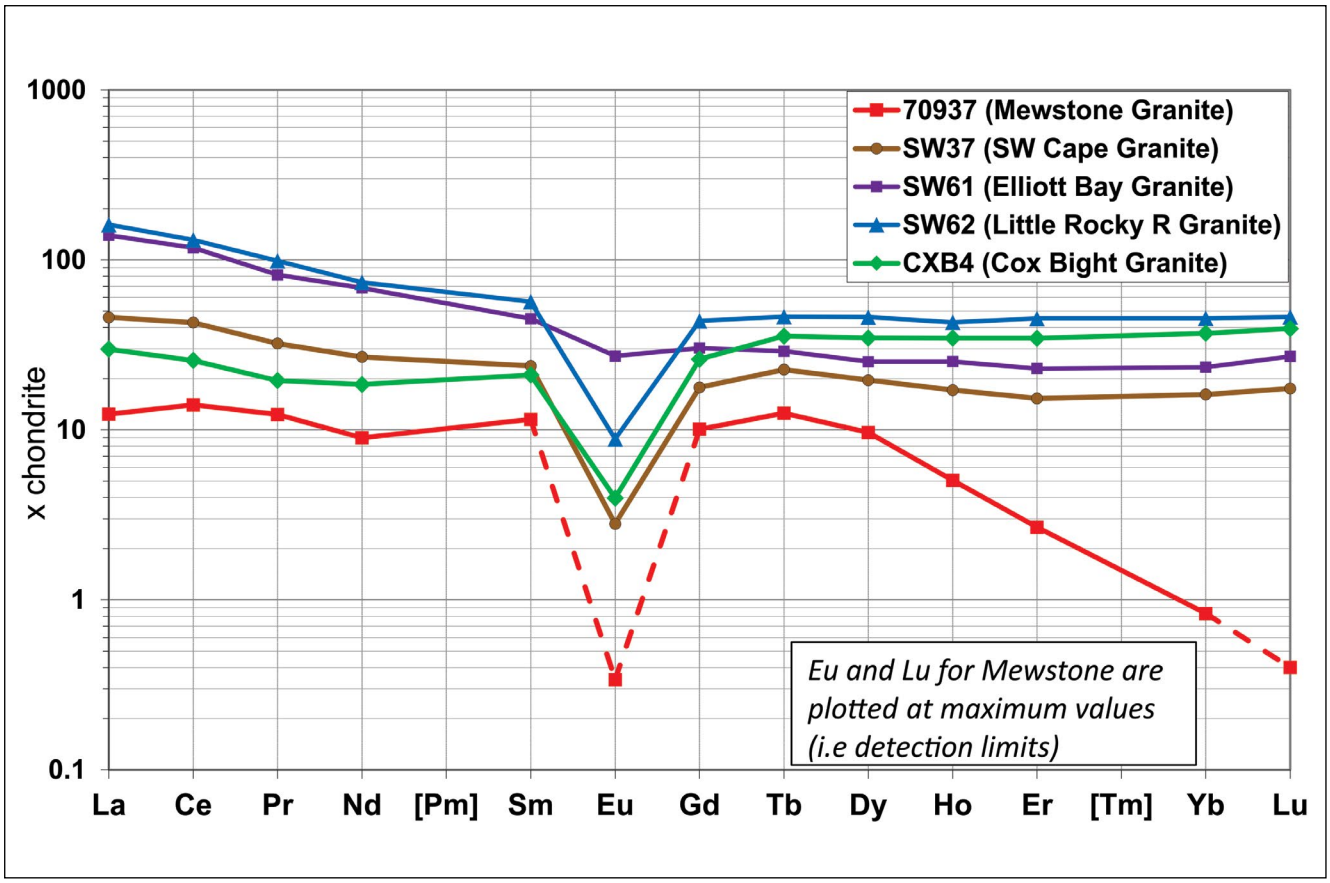

Figure 8. Chondrite-normalised rare-earth element plots for the Mewstone Granite, with other southwest Tasmanian Cambrian granites and Devonian Cox Bight Granite shown for comparison. C1 chondrite normalisation factors after O'Neill (2016).

is controlled by interaction with chemical complexes (possibly involving fluorine) in the aqueous fluid, rather than the charge and ionic radii ("CHARAC") controls of magmatic systems (e.g. Bau 1996; Irber 1999).

5.0 GEOCHRONOLOGY

Banks (1993) did not suggest an age for The Mewstone Granite. The lack of foliation perhaps suggests a post-Tabberabberan (i.e. Middle Devonian or younger) age, but the mesoscopic appearance of the granite is dissimilar to most Tasmanian Devonian granites.

The nearest granites on the Tasmanian mainland are the Cox Bight Granite and the South West Cape Granite. These had previously been dated by the Rb-Sr method at 376 ± 10 Ma and 319 ± 10 Ma respectively (C. Brooks, letter to Department of Mines, 14th June 1971). However, the more robust U-Pb SHRIMP method on zircon yielded 369.9 ± 2.5 Ma for the Cox Bight Granite, and 497.8 ± 3.3 Ma for the South West Cape Granite (Black et al. 2005). Whereas the ages obtained by differing methods are within error for the Cox Bight Granite, the much older Cambrian SHRIMP age for the South West Cape Granite suggests later resetting of the Rb-Sr system in this body. These contrasting Late Devonian and Late Cambrian SHRIMP ages also raised the question of the age of the Mewstone Granite.

5.1 U-Th-Pb on monazite

An attempt was made to determine the age of the Mewstone Granite using the chemical isochron method (CHIME) for monazite (e.g. Montel et al. 1996). This requires the determination of the U, Th and Pb contents from grains of magmatic monazite. If it can be assumed that the monazite contained no initial ("common") Pb when it crystallized, and that no Pb has been lost from the grain by secondary processes, all the Pb now present must be derived from radioactive decay of Th and U, and an age can be calculated for each grain.

Three polished thin sections (of samples 66272B, 66273B and 66270) were examined with the Cameca Electron Microprobe at the University of Tasmania (D. Steele, analyst). Attempts to identify magmatic monazites were made using a back-scattered electron image, which highlights minerals of high average atomic weight. Although numerous small (20-40 μm) grains of Th-rich phosphates were identified, most are irregular in shape, unlike typical magmatic monazites, and all were atypically high in Ca, Y, and heavy rare earth elements, depleted in light rare earths (especially La), and very low in Pb. Furthermore, some grains contain sulphur and totals were usually low, suggesting the presence of sulphate in addition to phosphate. It is concluded that the grains are secondary Th-Ca-Y-REE phosphates, probably derived from alteration of primary monazite. No meaningful age could be calculated, because of the likelihood of Pb loss, and the possibility of the presence of common Pb.

5.2 U-Pb on zircon

Eleven zircons extracted from sample 70937 were analysed by LA-ICPMS at the Central Science Laboratory, University of Tasmania. Methods and standards are described by Meffre & Thompson (2012). The analytical spot size was 32um.

Measured isotopic ratios included $^{207}Pb/^{206}Pb$, $^{206}Pb/^{238}U$ and $^{208}Pb/^{232}Th$. Three grains showed evidence of the presence of common Pb at the end of their analyses, one showed evidence of Pb loss in the latter part of the analysis, and a fifth grain showed both common Pb at the beginning and possible Pb loss at the end of its analysis. Six grains showed no evidence for either common Pb or Pb loss. Analytical results are given in Table 2 (Appendix 2).

Ages calculated from the $^{206}Pb/^{238}U$ ratio, using standard constants and uncorrected for common Pb, form a tight cluster ranging from 487 ± 5 to 507 ± 5 Ma (± 1σ).

On a concordia (Wetherill) plot of $^{206}Pb/^{238}U$ against $^{207}Pb/^{235}U$ (Fig. 9), seven grains plot on or very close to concordia, three show slight normal discordance (below the line) and the grain with both common Pb and possible Pb loss is more markedly discordant.

A similar pattern is seen on a reverse concordia (Tera-Wasserburg) plot of $^{207}Pb/^{206}Pb$ against $^{238}U/^{206}Pb$ (Fig. 10). The seven more-or-less concordant grains have (relatively imprecise) $^{207}Pb/^{206}Pb$ ages of 485 ± 29 to 544 ± 31 Ma, and the discordant grains have older $^{207}Pb/^{206}Pb$ ages ranging up to 1071 ± 78 Ma (± 1σ).

The $^{208}Pb/^{232}Th$ ages range from 354 ± 15 Ma to 629 ± 13 Ma (± 1σ), with a mean of ~487 ± 6 Ma and a weighted mean ($1/d^2$) of ~484 Ma.

A better estimate of the age of sample 70937, however, is considered to be obtainable from the $^{206}Pb/^{238}U$ ratios after correction for discordance, which it is assumed is due to the incorporation small amounts of common Pb (with $^{207}Pb/^{206}Pb$ of ~0.87 at ~500 Ma) during crystallisation of the zircons. For seven grains the correction is almost negligible (≤ 1 Myr). The estimated age of three grains is decreased by 2.1 to 4.5 Myr, whereas the age of the most discordant grain is decreased by ~11 Myr. The weighted ($1/d^2$) mean age of the eleven grains is 495.2 ± 5.0 Ma (2σ) (Fig 11).

The best estimate of the age of sample 70937, although not statistically different, is the lower intercept on Concordia (Fig, 12), calculated using IsoplotR (Ludwig 2012;Vermeesch 2008), which is **495.6 ± 5.2 Ma (2σ).**

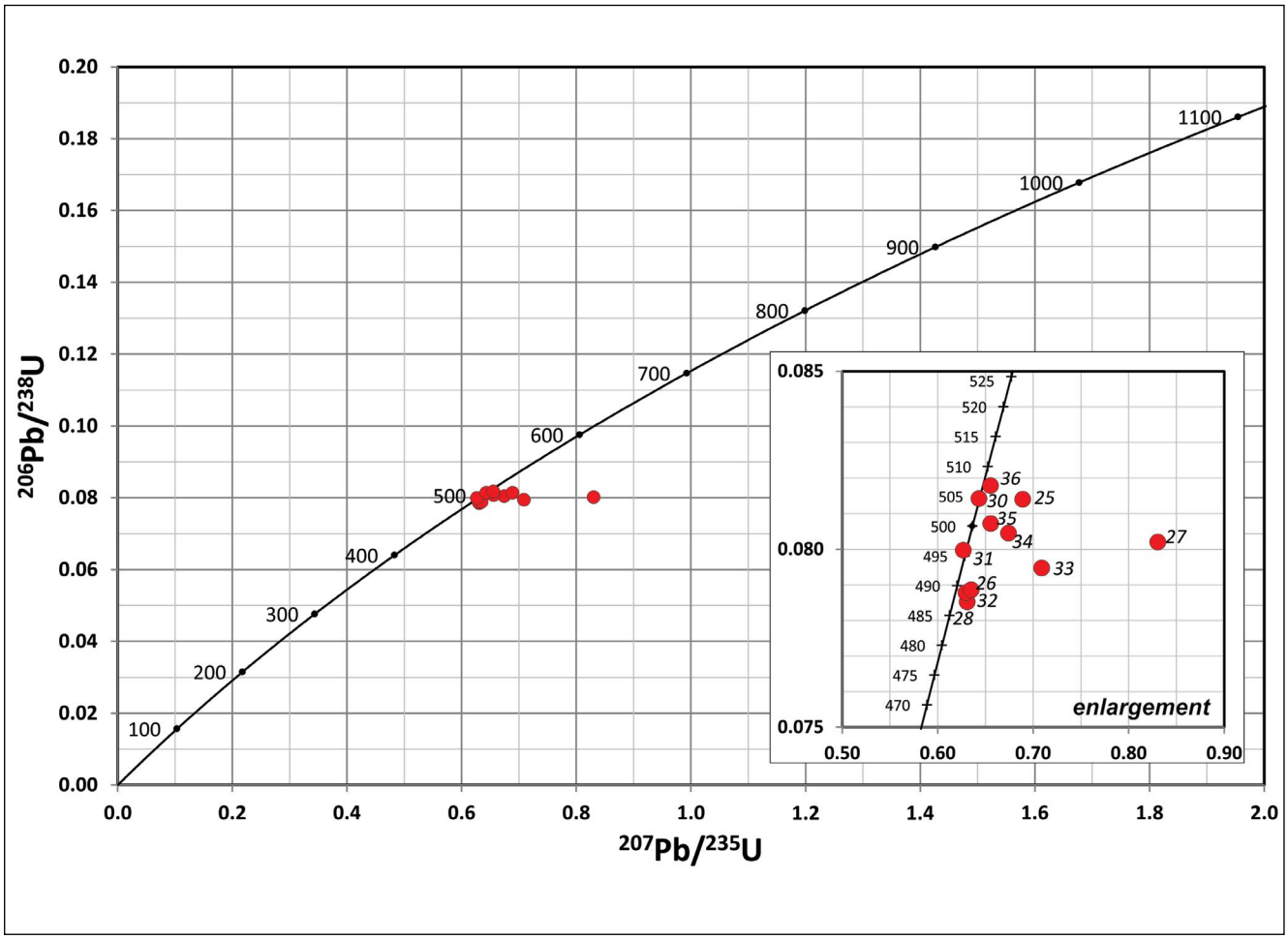

Figure 9. Concordia (Wetherill) plot of $^{206}Pb/^{238}U$ against $^{207}Pb/^{235}U$ for LA-ICPMS analyses of zircon grains from sample 70937; ticks on concordia show model ages in 100 Myr intervals. Inset shows detail at ~500 Ma with ages on concordia at 5 Myr intervals.

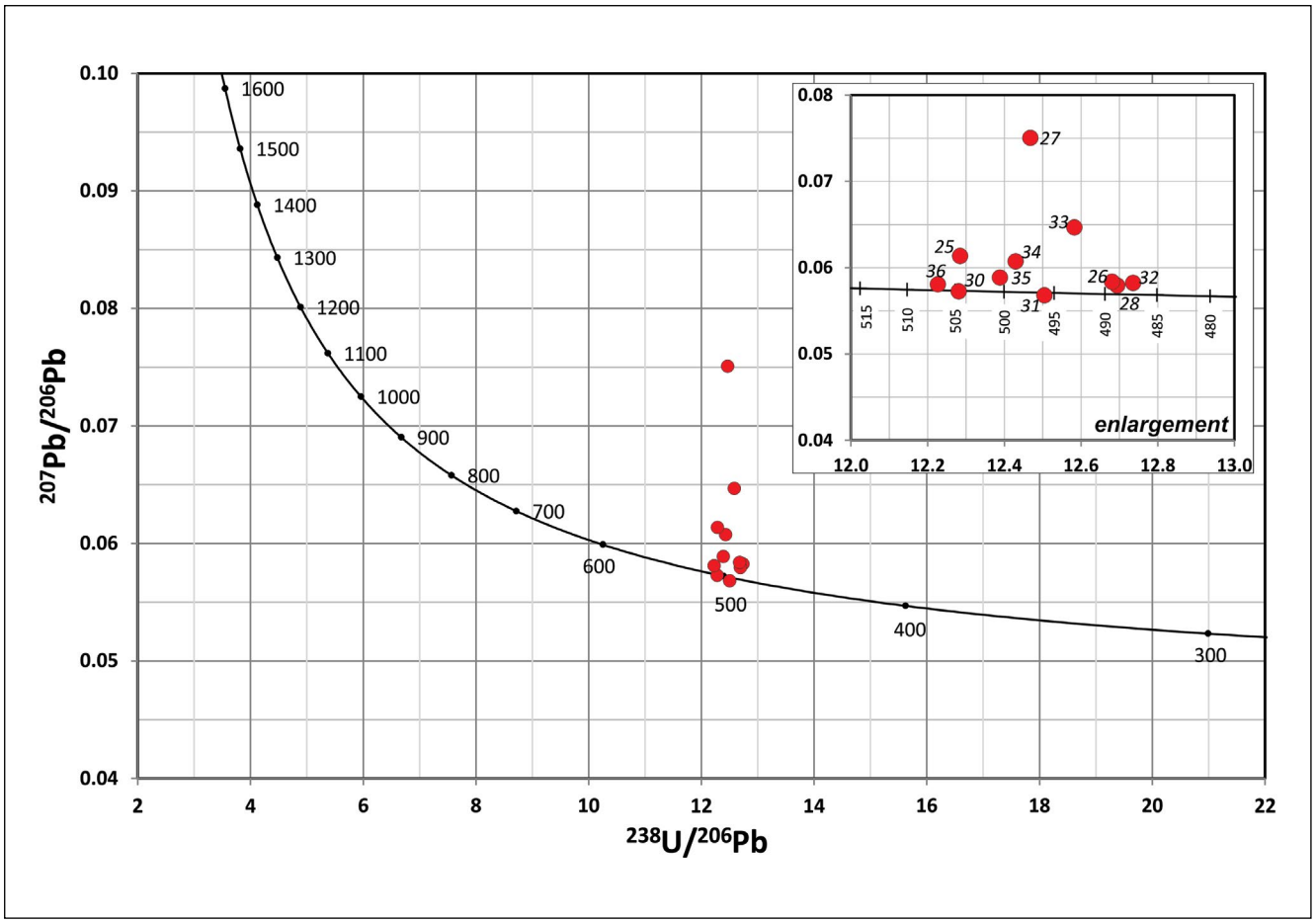

Figure. 10. Reverse concordia (Tera-Wasserburg) plot of $^{207}Pb/^{206}Pb$ against $^{238}U/^{206}Pb$ for LA-ICPMS analyses of zircon grains from sample 70937, inset shows detail at ~500 Ma.

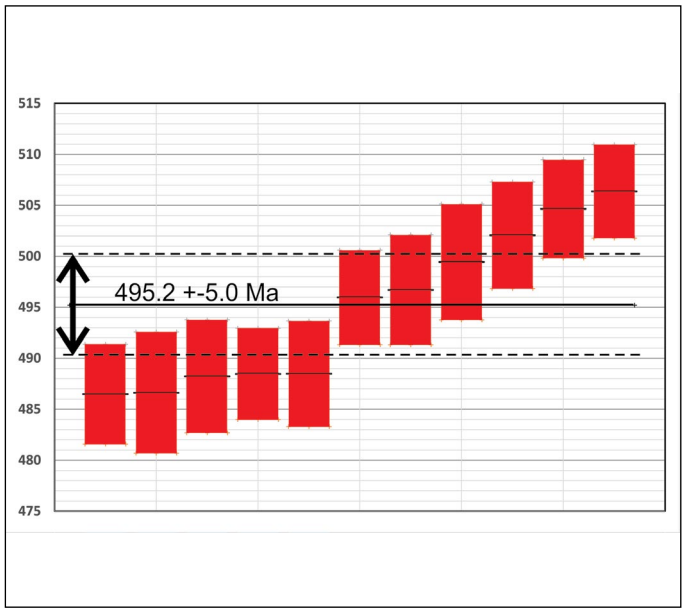

Figure 11. Histogram of ages of zircon grains derived from $^{206}Pb/^{238}U$ ratios with discordance removed by correction for common Pb ($^{207}Pb/^{206}Pb$ of ~0.87 at ~500 Ma), 1σ error bars shown. Arbitrary horizontal axis with analyses arranged in order of increasing age.

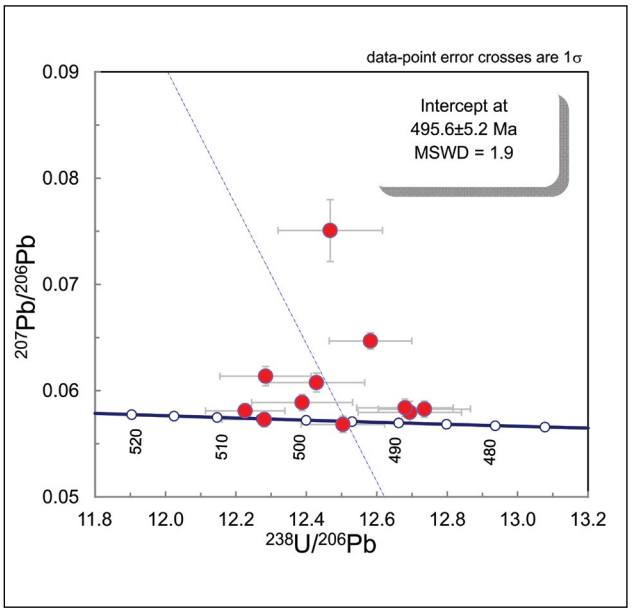

Figure 12. Reverse concordia plot of $^{207}Pb/^{206}Pb$ against $^{238}U/^{206}Pb$, showing error bars and best fit line from common Pb; intercept with concordia gives preferred age estimate for sample 70937. Plotted using Isoplot software (Ludwig 2012, Vermeesch 2018).

6.0 DISCUSSION AND CONCLUSION

This age is Cambrian (Furongian) according to the most recent International Stratigraphic Chart (Cohen et al. 2022), although it is well within error of the Furongian-Miaolingian boundary at ~497 Ma (i.e. Late Cambrian- Early Cambrian of older terminology).

The Cambrian age of the Mewstone Granite precludes any relationship to the Devonian Cox Bight Granite (369.9 ± 2.5 Ma, U-Pb SHRIMP; Black et al., 2005), despite some similarities in composition. However, it is within error of the South West Cape Granite (497.8 ± 3.3 Ma, U-Pb SHRIMP; Black et al. 2005). The South West Cape Granite is also similar in its highly felsic, strongly peraluminous composition. The Mewstone Granite has lower CaO, Y and REE, slightly lower Na_2O, and higher K_2O and P_2O_5 (Table 1; Appendix 1). The pattern displayed by the LREE and MREE has some resemblance, at lower absolute levels, to that of the Cambrian South West Cape Granite, but the HREE (from Ho to Lu) are much more depleted (Fig. 8). These differences reflect both the stronger fractionation of the Mewstone Granite and the effects of hydrothermal alteration and possibly weathering.

Farther afield, similar but higher precision Cambrian ages have been obtained from outcropping granites in the Elliott Bay-Low Rocky Point area (Little Rocky River Granite, 497.0 ± 0.6 Ma; Elliott Bay Granite, 497.7 ± 0.4 Ma) by the U-Pb chemical abrasion/thermal ion mass spectroscopy method (Mortensen et al. 2015). The latter compares with a less precise U-Pb SHRIMP age of 498.8 ± 3.3 Ma (Black et al. 2005). However, these granites are distinctly less peraluminous (i.e. have lower ASI) than either the Mewstone or South West Cape Granites, and the Elliott Bay Granite in particular appears to be less fractionated, with lower Rb and higher Sr, Ba and Zr (Table 1; Appendix 1). In the I/S granite classification, the Elliott Bay and Little Rocky River Granites would be termed I-types (i.e. derived from a predominantly igneous or infracrustal protolith).

It is probably significant that the South West Cape Granite intrudes the much older Mesoproterozoic metasedimentary rocks of the Tyennan Region, whereas the Elliott Bay and Little Rocky River Granites (together with other Cambrian granites further north such as the Murchison and Darwin Granites) have intruded Cambrian volcanic sequences (Mt Read Volcanics, mainly the Eastern Quartz-phyric Sequence) of the "Dundas Trough", which are not much older (~498 – 502 Ma) than the granites themselves (Mortensen et al., 2015; Vicary et al., 2015). The country rock of the Mewstone Granite is unknown, but it lies well to the east of the southward extrapolation of the Mt Read Volcanics and Dundas Trough.

In a wider tectonic context, the Proterozoic sedimentary rocks of the western Tasmanian microcontinent (Tyennan region) probably collided with an east-dipping oceanic arc at ~506 Ma (Miaolingian, i.e. Middle Cambrian) resulting in westward obduction of oceanic sediments, mafic volcanics and complementary cumulates (e.g. Berry & Crawford, 1988; Berry, 2014). Post-collisional uplift of the Tyennan Region was accompanied by felsic volcanism (Mt Read Volcanics), peaking at ~500 Ma (e.g. Mortensen et al., 2015). The waning stages of this volcanism (Tyndall Group and correlates) continued until ~493 Ma and were accompanied by intrusion of sub-volcanic granites, mainly into the young volcanic pile (Mortensen et al., 2015; Vicary et al., 2015).

The Mewstone and South West Cape Granites may present a distal phase of this plutonism, in which related arc-granite magmas, contaminated by assimilation of old sedimentary material, were emplaced into the adjacent uplifted Proterozoic rocks of the old continental basement. However, the precision of the dates from both bodies is insufficient to constrain the exact timing of events.

7.0 ACKNOWLEDGEMENTS

Samples from the Mewstone were obtained from the rock collection of the Department of Natural Sciences (Earth Sciences), University of Tasmania. Micah Visoui (Department of Natural Resources and Environment) supplied field photographs. MRT technical staff prepared thin sections and whole rock (XRF) analyses. Rare earth element data were part of a larger batch analysed at Geoscience Australia, courtesy of David Champion. Geochronological analyses were by Jay Thompson (University of Tasmania). A. McNeill critically reviewed the manuscript, which was prepared for publication by C. Large.

8.0 REFERENCES

Banks, M. R. 1993. *Reconnaissance geology and geomorphology of the major islands south of Tasmania*. Tasmania Department of Parks, Wildlife and Heritage.

Bau, F. 1996. Controls on the fractionation of isovalent trace elements in magmatic and aqueous systems: evidence from Y/Ho, Zr/Hf and lanthanide tetrad effect. *Contributions to Mineralogy and Petrology* 80, 189-200.

Berry, R. F. 2014. Cambrian tectonics- the Tyennan Orogeny. IN: Corbett K.D., Quilty P.G. & Calver C.R. (EDS.) *Geological Evolution of Tasmania. Special Publication,* 24, Geological Society of Australia, p. 95-110.

Berry, R. F. and Crawford, A. J. 1988. The tectonic significance of Cambrian allochthonous mafic – ultramafic complexes in Tasmania. *Australian Journal of Earth Sciences,* 35, 523-533.

Black, L. P., McClenaghan, M. P., Korsch, R. J., Everard, J. L. & Foudoulis, C. 2005. The significance of Devonian-Carboniferous igneous activity in Tasmania, as derived from U-Pb SHRIMP dating of zircon. *Australian Journal of Earth Sciences,* 52, 807-829.

Brothers, N., Pemberton, D., Pryor, H. and Halley, V. 2001. *Tasmania's Offshore Islands: seabirds and other natural features*. Tasmanian Museum and Art Gallery, Hobart.

Chappell, B. W. 1999. Aluminium saturation in I- and S-type granites and the characterization of fractionated haplogranites. *Lithos*, 46 (3), 535-551.

Chappell, B. W. and White, A. J. R. 1974. Two contrasting granite types. *Pacific Geology*, 8: 173-174.

Chappell, B. W. and White, A. J. R. 1992. I- and S-type granites in the Lachlan Fold Belt. *Transactions of the Royal Society of Edinburgh: Earth Sciences*, 83: 1-26.

Cohen, K. M., Finney, S. C., Gibbard, P. L. & Fan, J.-X. 2013, updated 2022. The ICS International Chronostratigraphic Chart. *Episodes*, 36, 159-204.

Irber, W. 1999. The lanthanide tetrad effect and its correlation with K/Rb, Eu/Eu*, Sr/Eu, Y/Ho and Zr/Hf of evolving peraluminous granite suites. *Geochimica et Cosmochimica Acta*, 63, 489-508.

Ludwig, K. 2012. User's Manual for Isoplot 3.75. A Geochronological Toolkit for Microsoft Excel. *Special Publication,* 5, Berkeley Geochronology Center, Berkeley, California 75.

McLennan, S. M. 1994. Rare earth geochemistry and the "tetrad" effect. *Geochimica et Cosmochimica Acta*, 58, 2025-2033.

Masuda, A., Kawakami, O., Dohmoto, Y. and Takenaka, T. 1987. Lanthanide tetrad effects in nature. Two mutually opposite types, W and M. *Geochemical Journal*, 21, 119-124.

Meffre, S. and Thompson, J. 2012. LA-ICPMS zircon geochronology at the University of Tasmania (unpublished).

Montel, J.-M. 1986. Experimental determination of the solubility of Ce-monazite in SiO_2-Al_2O_3-K_2O-Na_2O melts at 800C, 2 kbar, under H_2O-saturated conditions. *Geology*, 14: 659-662.

Montel, J.-M., Foret, S., Veschambre, M., Nicollet, C. and Provost A. 1998. Electron microprobe dating of monazite. *Chemical Geology*, 131, 37-53.

Mortensen, J. K., Gemmell, J. B., McNeill, A. W. and Friedman, R.M. 2015. High precision U-Pb zircon chronostratigraphy of the Mt Read Volcanic belt in western Tasmania, Australia: implications for VHMS deposit formation. *Economic Geology*, 110, 443-468.

O'Neill, H., St. C. 2016. The smoothness and shapes of chondrite-normalized rare earth element patterns in basalts. *Journal of Petrology*, 57, 1463-1508.

Pichavant, M., Montel, J.-M. and Richard, L. R. 1992. Apatite solubility in peraluminous liquids: experimental data and an extension of the Harrison-Watson model. *Geochimica et Cosmochimica Acta*, 56: 3855-3861.

Sawka, W. N., Heizler, M. T., Kistler, R. W. and Chappell, B. W. 1990. Geochemistry of highly fractionated I- and S-type granites from the tin-tungsten province of western Tasmania. In: Stein, H. J. & Hannah, J. L. (EDS.). Ore- bearing granite systems: petrogenesis and mineralising processes. *Geological Society of America Special Paper*, 246, 161-179.

Vermeesch, P. 2018. IsoplotR, a free and open toolbox for geochronology. *Geoscience Frontiers*, 9, 1479-1493. doi: 10.1016/j.gsf.2018.04.001.

Vicary, M. J., Mortensen, J. K., McNeill, A. W., Gemmell, J. B. and Friedman, R.M. 2015. High precision U-Pb chronostratigraphy of the Mount Read Volcanic belt in western Tasmania, Australia: new results and implications for VHMS exploration. Poster, Society of Economic Geologists Discovery to Recovery Conference, Hobart (unpublished).

Wolf, M. B. and London, D. 1994. Apatite dissolution into peraluminous haplogranitic melts: an experimental study of solubilities and mechanism. *Geochimica et Cosmochimica Acta*, 58: 4127-4145.

Wyborn, D. and Chappell, B. W. 1998. Compositional changes during fractionation of felsic granites from western Tasmania, Australia. Acta Universitas Carolinae, *Geology*, 42, 189-193.

APPENDIX 1

Located :

https://www.mrt.tas.gov.au/mrtdoc/dominfo/download/TR33/

Appendix 1 - Whole rock analyses of the Mewstone Granite and other southwest Tasmanian granites

-Download-

Table 1. Whole rock analyses of the Mewstone Granite and other southwest Tasmanian granites.

Mewstone Granite					**South West Cape Granite**						
Field No.	-	-	-		**SW37**	**SW37**	**SW36**	**SW48**	**SWC1**	**SWC2**	**SWC3**
Reg No	70937	70937	70937		R011515	R011515	R011521	R011523	R004453	R004454	R004455
lab	MRT	GA	GA		GA	MRT	MRT	MRT	MRT	MRT	MRT
Anal No.	20040125	1950965	1950965		2002220086	20030076	20030079	20030080	20010183	20010184	20010185
SiO_2 (%)	76.53	75.77			77.16	76.37	75.30	75.89	75.83	76.42	75.54
TiO_2	0.10	0.10			0.15	0.10	0.07	0.08	0.12	0.08	0.07
Al_2O_3	12.43	12.45			13.10	12.94	13.69	13.26	13.17	12.99	13.53
Fe_2O_3	0.63	1.19			0.07	0.29	0.36	0.41	0.03	0.29	0.26
FeO	0.58	nd			1.00	0.97	0.97	0.71	1.35	0.77	0.70
MnO	0.00	<0.005			0.03	0.03	0.01	0.03	0.03	0.03	0.02
MgO	0.01	0.07			0.20	0.12	0.05	0.09	0.29	0.24	0.17
CaO	0.09	0.06			0.37	0.35	0.24	0.34	0.49	0.21	0.42
Na_2O	2.30	2.68			3.02	2.91	3.00	2.94	2.98	2.54	3.25
K_2O	5.77	5.70			4.74	4.77	5.13	5.15	4.60	5.58	4.91
P_2O_5	0.39	0.45			0.11	0.06	0.14	0.06	0.09	0.06	0.18
SO_3	0.01	0.02			0.03	0.00	0.01	0.00	0.03	0.02	0.02
LOI		1.43			0.03						
O Equiv					-0.03						
Rest					0.07						
CO2	0.07					0.10	0.10	0.08	0.14	0.14	0.05
H2O+	0.81					0.61	0.72	0.63	0.72	0.60	0.70
Total	**99.71**	**99.93**			**100.07**	**99.62**	**99.79**	**99.66**	**99.86**	**99.98**	**99.80**
MLOI Calc	0.82				-0.099	0.60	0.71	0.63	0.71	0.66	0.77
FeOtot	1.15	1.07			1.06	1.23	1.30	1.08	1.38	1.03	0.93
ASI	1.219	1.164			1.218	1.222	1.254	1.202	1.223	1.225	1.185
			(ICPMS)								
Be (ppm)		1.2			4.9						
F					723						
Sc	<9	1	1		6	<9	<9	<9	<9	<9	<9
V	<5	<1	1.6		5	6	5	<5	0	13	11
Cr	5		5		<2	<5	8	10	<5	<5	<5
Co	<8	<1	0.6		nd	<8	<8	<8	<8	<8	<8
Ni	5	3	15.0		9	6	5	5	<5	<5	5
Cu	7	4	4.2		4	8			5	5	5
Zn	23	27	25.3		26	15	23	15	18	12	19
Ga	19	20.4	20.8		18	17	20	18	16	16	20
Ge			1.6		2.3						
As	<20	2.4	1.4		0.6	<20	<20	<20	<20	<20	<20
Rb	310	310.8	310.6		337.2	340	440	320	250	290	420
Sr	10	14.1	13.2		31.2	16	8	16	32	14	9
Y	18	14	11.3		25.8	32	33	32	31	27	28
Zr	63	69	63.6		55	55	45	58	72	67	45
Nb	14	16	16.3		11.6	8	14	8	9	8	15
Mo	<5	2	2.2		0.9	<5	<5	<5	<5	<5	<5
Ag			<0.6		0.03						
Cd			<0.02		0.17						
Sn	<9		6.8		7	19	<9	<9	<9	<9	<9
Sb			<0.8		0.2						
Cs		5	5.5		13.04						
Ba	32	27	29.3		66	82	40	87	135	<23	36
La		<5	3.06		11.36	<20	<20	<20	<20	<20	<20
Ce		<8	8.9		26.98	<28	<28	30	29	<28	<28
Pr			1.17		3.06						
Nd		8	4.31		12.87	<20	<20	<20	<20	<20	<20
Sm			1.78		3.67						
Eu			<0.02		0.166						
Gd			2.08		3.66						
Tb			0.47		0.85						
Dy			2.45		4.98						
Ho			0.28		0.95						
Er			0.44		2.52						
Yb			0.14		2.72						
Lu			<0.01		0.44						
Hf			2.83		2.6						
Ta			1.14		2.5						
W	<10	8	3.1			16	<10	<10	<10	<10	<10
Pb	12	16	15.1		20.9	18	21	22	22	19	19
Bi	<5	<1	0.25		0.1	<5	<5	<5	<5	<5	<5
Th	<10	9	8.8		8.7	<10	<10	<10	<10	<10	<10
U	<10	2.8	2.26		2.98	<10	<10	<10	<10	<10	<10
FeO_{tot} is total iron expressed as FeO											

Cox Bight Granite						Elliott Bay Granite		L Rocky R
Field No.	**CXB4**	**CXB4**	**CXB1**	**CXB2**		**SW61**	**SW61**	**SW62**
Reg No	R011514	R011514	R004456	R004457		R011516	R011516	R0011517
lab	GA	MRT	MRT	MRT		GA	MRT	MRT
Anal No.	2002220085	20030075	20010186	20010187		2002220087	20030077	20030078
SiO2 (%)	75.10	74.18	74.03	76.09		75.63	75.41	77.45
TiO_2	0.22	0.19	0.20	0.11		0.24	0.20	0.12
Al_2O_3	13.83	13.96	14.04	13.37		12.91	12.75	11.84
Fe_2O_3	0.26	0.391	0.20	0.20		1.11	0.96	0.59
FeO	1.00	1.29	1.47	0.45		0.73	0.90	0.58
MnO	0.06	0.07	0.07	0.03		0.02	0.01	0.01
MgO	0.39	0.51	0.55	0.28		0.29	0.23	0.03
CaO	1.13	1.15	1.14	0.43		1.16	1.11	0.24
Na_2O	3.58	3.67	3.80	3.18		2.97	2.96	2.29
K_2O	3.86	3.69	3.47	4.92		4.61	4.49	5.97
P_2O_5	0.07	0.04	0.07	0.05		0.06	0.01	0.00
SO3	0.04	0.01	0.02	0.02		0.03	0.01	0.01
LOI	0.42					0.13		
O Equiv	-0.03					-0.02		
Rest	0.10					0.18		
CO_2		0.08	0.11	0.19			0.09	0.09
H2O+		0.64	0.68	0.58			0.60	0.58
Total	**100.06**	**99.86**	**99.84**	**99.90**		**100.05**	**99.74**	**99.79**
MLOI Calculate	0.282	0.57	0.62	0.72		0.027	0.59	0.60
FeOtot	1.23	1.64	1.65	0.63		1.73	1.76	1.11
ASI	1.142	1.151	1.163	1.180		1.077	1.084	1.110
Be (ppm)	10.6					2.7		
F	579					415		
Sc	7	<9	<9	<9		6	<9	<9
V	14	16	22	17		13	16	<5
Cr	6	11	<5	<5		<2	12	9
Co		<8	<8	<8			<8	<8
Ni	14	6	6	5		12	6	6
Cu	5	8	6	15		6	10	20
Zn	35	34	36	8		20	10	6
Ga	18	18	18	17		14.5	15	15
Ge	2.7					1.5		
As	1.6	<20	<20	<20		0.8	<20	<20
Rb	446.7	460	430	380		142.7	135	310
Sr	66.1	56	56	24		138.6	130	24
Y	73.1	100	99	83		37.4	44	74
Zr	86	105	100	74		175	145	135
Nb	15.4	16	18	13		17.3	15	27
Mo	1.1	<5	<5	<5		2.9	<5	6
Ag	0.03					0.03		
Cd	<0.1					0.14		
Sn	19.8	21	13	9		2.5	13	<9
Sb	0.2					0.2		
Cs	30.41					1.09		
Ba	160	175	170	97		939	970	93
La	9.26	<20	<20	<20		34.52	<20	46
Ce	20.72	<28	30	<28		74.4	<20	95
Pr	2.38					7.76		32
Nd	11.1	<20	<20	<20		32.81	<20	
Sm	4.11					6.96		
Eu	288					1610		
Gd	6.75					6.24		
Tb	1.69					1.09		
Dy	11.18					6.4		
Ho	2.49					1.4		
Er	7.26					3.78		
Yb	7.74					3.94		
Lu	1.27					0.68		
Hf	3.8					6		
Ta	4.9					1.4		
W		<10	<10	<10			<10	<10
Pb	37.9	36	29	40		5.8	<10	<10
Bi	2.5	<5	<5	10		-0.1	<5	<5
Th	14.2	18	16	23		30.7	21	46
U	7.2	11	10	15		4.75	<10	30
FeO_{tot} is total iron expressed as FeO								

APPENDIX 2

Located :

http://www.mrt.tas.gov.au/mrtdoc/dominfo/download/TR33/

Appendix 2 - Geochronological data, LA-ICPMS analyses of zircon grains

-Download-

Table 2. Geochronological data, LA-ICPMS analyses of zircon grains.

Sample 70937			Ages										
			207cor $^{206}Pb/^{238}U$		$^{206}Pb/^{238}U$		$^{208}Pb/^{232}Th$		$^{207}Pb/^{206}Pb$		$^{206}Pb/^{238}U$		
Session	Analysis	No.	age (Ma)	±1 SE	age (Ma)	±1 SE	age (Ma)	±1 SE	age (Ma)	±1 SE	ratio	± RSE	Comment
2013-309	JL23B032	32	486.49	4.90	487.30	4.99	466.3	9.3	539.7	29.0	0.0785	1.0%	ok
2013-309	JL23B027	27	486.63	5.94	497.36	5.93	458.1	17.3	1070.5	78.0	0.0802	1.2%	common Pb @ beginning, Pb loss @ end?
2013-309	JL23B026	26	488.23	5.55	488.83	5.65	354.5	14.6	528.1	39.6	0.0788	1.2%	Pb loss in 2nd half
2013-309	JL23B033	33	488.47	4.47	493.00	4.59	629.3	12.8	764.1	25.1	0.0795	0.9%	ok
2013-309	JL23B028	28	488.48	5.18	489.33	5.29	507.1	10.4	544.3	30.5	0.0789	1.1%	ok
2013-309	JL23B031	31	495.97	4.64	495.97	4.72	510.5	12.1	484.9	29.2	0.0800	1.0%	ok
2013-309	JL23B034	34	496.71	5.39	498.86	5.51	542.9	14.9	630.8	31.2	0.0805	1.1%	common Pb @ end
2013-309	JL23B035	35	499.45	5.68	500.44	5.80	421.7	10.7	562.9	28.5	0.0807	1.2%	Common Pb @ end
2013-309	JL23B025	25	502.07	5.21	504.51	5.33	530.1	13.2	652.0	32.0	0.0814	1.1%	common Pb @ end
2013-309	JL23B030	30	504.65	4.84	504.65	4.94	510.4	11.4	502.2	26.7	0.0814	1.0%	ok
2013-309	JL23B036	36	506.37	4.58	506.80	4.67	424.0	10.3	533.6	26.3	0.0818	0.9%	ok

			Ratios									
			$^{208}Pb/^{232}Th$		$^{207}Pb/^{206}Pb$			$^{238}U/^{206}Pb$		206/207 common Pb		
Session	Analysis	No.	ratio	± RSE	ratio	±1 SE	%SE	ratio	±1 SE	at age of zircon		
2013-309	JL23B032	32	0.0233	2.0%	0.0583	0.0008	1.3%	12.74	0.13	0.869		
2013-309	JL23B027	27	0.0229	3.8%	0.0751	0.0029	3.9%	12.47	0.15	0.870		
2013-309	JL23B026	26	0.0177	4.1%	0.0580	0.0010	1.8%	12.69	0.15	0.869		
2013-309	JL23B033	33	0.0316	2.0%	0.0647	0.0008	1.2%	12.58	0.12	0.869		
2013-309	JL23B028	28	0.0254	2.1%	0.0584	0.0008	1.4%	12.68	0.14	0.869		
2013-309	JL23B031	31	0.0256	2.4%	0.0568	0.0008	1.3%	12.50	0.12	0.869		
2013-309	JL23B034	34	0.0272	2.7%	0.0608	0.0009	1.5%	12.43	0.14	0.870		
2013-309	JL23B035	35	0.0211	2.5%	0.0589	0.0008	1.3%	12.39	0.14	0.870		
2013-309	JL23B025	25	0.0266	2.5%	0.0614	0.0009	1.5%	12.28	0.13	0.870		
2013-309	JL23B030	30	0.0256	2.2%	0.0573	0.0007	1.2%	12.28	0.12	0.870		
2013-309	JL23B036	36	0.0212	2.4%	0.0581	0.0007	1.2%	12.23	0.11	0.870		

			Element (ppm)								
			^{204}Pb	^{206}Pb	^{207}Pb	^{208}Pb	^{232}Th	^{238}U	^{49}Ti	^{56}Fe	^{178}Hf
Session	Analysis	No.	ppm	ppm	ppm	ppm	ppm	ppm	ppm	ppm	ppm
2013-309	JL23B032	32	0.00	43.99	2.56	1.70	73.29	574.25	41.02	483.62	14913
2013-309	JL23B027	27	0.06	59.09	4.26	4.60	205.33	765.85	253.86	317.29	14885
2013-309	JL23B026	26	0.02	47.05	2.74	1.70	105.44	654.62	5.98	331.72	15932
2013-309	JL23B033	33	0.06	64.22	4.15	3.14	101.25	832.11	4.90	169.00	15357
2013-309	JL23B028	28	0.00	32.51	1.88	1.61	65.32	428.69	7.10	5.26	14689
2013-309	JL23B031	31	0.00	45.31	2.57	1.26	49.96	582.85	7.54	95.77	15544
2013-309	JL23B034	34	0.01	67.25	4.10	2.57	99.04	900.84	27.21	893.68	16073
2013-309	JL23B035	35	0.02	59.29	3.51	2.75	137.99	786.03	6.43	82.18	15422
2013-309	JL23B025	25	0.00	44.84	2.78	2.35	88.07	577.75	6.57	4.03	14772
2013-309	JL23B030	30	0.00	46.28	2.63	1.38	54.99	583.68	3.56	2.96	15860
2013-309	JL23B036	36	0.00	60.93	3.54	1.59	75.08	768.69	6.14	11.80	15960

Tasmanian
Government

Mineral Resources Tasmania
PO Box 56 Rosny Park
Tasmania Australia 7018
Ph: +61 3 6165 4800

info@mrt.tas.gov.au www.mrt.tas.gov.au